

Dispersion in One-Dimensional Photonic Band Gap Periodic Transmission Lines

C. Isaac Angert^{1,2} and Stephen K. Remillard¹

¹Physics Department, Hope College, Holland, MI, 49423 USA, corresponding author.

²Physics Department, Truman State University, Kirksville, MO, 63501 USA

Abstract—Dispersion in periodic microstrip transmission lines was investigated by using S-parameters to calculate the characteristic impedance and the complex propagation constant. Dispersion curves determined from a variety of methods, including simulation with IE3D and measurement with a network analyzer, were compared to an analytic transcendental model providing self-consistent validation of each method. Simulated S-parameters agreed with measurement, including the case of a multi-layered substrate. Very similar dispersion curves were produced using simulated S-parameters, simulated current distributions, analytic calculation and measured S-parameters.

Keywords: Periodic Transmission Line; Transmission Line; Photonic Band Gap; Brillouin Zone; Dispersion

I. INTRODUCTION

Signal transmission through a periodic transmission line exhibits a broad rejection band, or a photonic band gap (PBG), across a frequency range which is commensurate with the spatial periodicity of structural irregularities in the transmission lines. Both transverse-electric-and-magnetic (TEM) microstrip transmission lines and non-TEM waveguides exhibit transmission with a PBG. This work is concerned with quasi TEM mode transmission lines so that the frequency response includes low frequencies, all the way down to DC.

The peculiar frequency response in the transmission characteristic is accompanied by a transmission line dispersion that is affected by the periodicity in the wave impedance. After the work by Kee¹ ten years ago linking the PBG directly to the periodicity in transmission line characteristic impedance, workers began to focus attention on dispersion engineering², creating a striking parallel between electromagnetic wave propagation along a periodic transmission line, and nearly free electron propagation through the periodic potential of a crystal lattice. The work reported here was, in fact, motivated by the possibility of developing an effective hands-on pedagogical tool to teach the band theory of solids.

Two microstrip line styles that were employed in this work are shown in Figure 1. The periodic variations in impedance were realized either by placing square holes in the strip, or by varying the width of the strip. The S-parameters of the lines

were measured, and the characteristic impedance and propagation constants were calculated. Measured results were found to be in very good agreement with numerical simulation.

A microstrip line on a homogeneous dielectric substrate of relative permittivity, ϵ_s , with air above the line has a characteristic impedance corresponding to the customarily used expression for effective dielectric constant³

$$\epsilon_{eff} \approx \frac{\epsilon_s + 1}{2} + \frac{\epsilon_s - 1}{2\sqrt{1 + 12(h/w)}} \quad (1)$$

where h and w are the substrate thickness and line width respectively, and $w > h$. This expression could be applied to the simple transmission lines used in this work; however in the first several lines fabricated here, a multilayer substrate was accidentally achieved. Although most structures were patterned on Rogers RO3003⁴, some of the structures were fabricated on either PTFE ($\epsilon_r \approx 2.2$) or on CoorstekTM 99.5% alumina ($\epsilon_r \approx 9.8$) substrates. The ground planes and microstrip lines were cut from acrylic adhesive backed copper tape⁵ using a razor blade. The approximately 60 μm thick adhesive layer on the tape reduced ϵ_{eff} by about 30% to 35%, significantly altering the PBG frequency response.

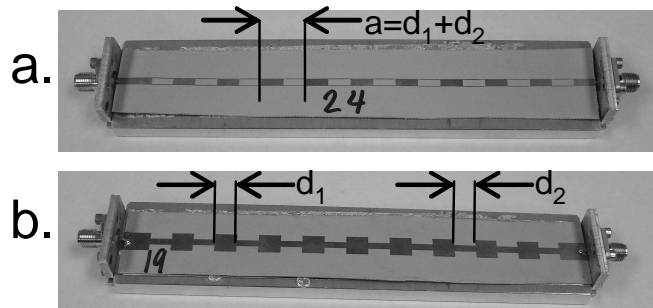


Figure 1 Periodic transmission lines (a) with holes and (b) with variations in line width. Each board is 15 cm long.

In the case of a lossless periodic transmission line, the propagation constant is real and constrained by the inequality⁶

$$\left| \cos(k_1 d_1) \cos(k_2 d_2) - \frac{1}{2} \left(\frac{Z_2 + Z_1}{Z_1} + \frac{Z_1}{Z_2} \right) \sin(k_1 d_1) \sin(k_2 d_2) \right| \leq |\cos(\beta a)| \quad (2)$$

where Z_1 and Z_2 are the characteristic impedance in the regions

with propagation constants $k_1 = \omega\sqrt{\epsilon_{1eff}}/c$ and $k_2 = \omega\sqrt{\epsilon_{2eff}}/c$. $\beta=2\pi/\lambda$ is the effective wave number for a wave propagating through the entire crystal, and c is the speed of light in vacuum. This expression is the usual quantum mechanical transcendental result for the Schrödinger equation with a Kronig-Penny potential⁷ using purely real propagation constants. The case of equality in Equation 2 defines the band edges, and wave numbers cannot exist if the left hand side of Equation 2 is greater than unity. d_1 and d_2 are the lengths of each section. Equation 2 is useful to qualitatively predict the upper and lower edges of the band gap. It fails in precise prediction possibly due to the frequency dependence of the impedance, especially near the band edges where the line is extremely dispersive.

The complex impedance, Z , and complex propagation coefficient, $\alpha+j\beta$, of a periodic transmission line can be calculated from the measured magnitude and phase of the S-parameters using the de-embedding equations used by Eisenstadt and Eo⁸ for IC interconnect characterization,

$$Z^2 = Z_o^2 \frac{(1 + S_{11})^2 - S_{21}^2}{(1 - S_{11})^2 - S_{21}^2} \quad (3)$$

and

$$e^{j(\alpha+j\beta)L} = \frac{1 - S_{11}^2 + S_{21}^2 + \sqrt{(1 + S_{11}^2 - S_{21}^2)^2 - (2S_{11})^2}}{2S_{21}} \quad (4)$$

where S_{11} and S_{21} are complex, L is the physical length of the transmission line in meters, α is the attenuation constant in Np/m and β is the propagation constant in m^{-1} . Z_o is the system impedance, and in these measurements $Z_o=50 \Omega$. These expressions have subsequently been used by others working on periodic transmission lines to extract the transmission line parameters from the measured S-parameters^{9,10}.

II. PERIODIC TRANSMISSION LINE CHARACTERIZATION

Two microstrip line structures were studied here and are shown in Figure 1. A patterned line with rectangular holes periodically spaced with period $a=14$ mm in the top metal layer is shown in Figure 1(a). Variations on this structure were studied in [1] by fabricating a suspended air dielectric metal line with holes, by Saib, et al.¹¹ by patterning the holes in the substrate and placing a straight transmission line on top, and by Tiwari¹², et al by cutting the structure from aluminum foil and placing it on top of a dielectric. Figure 1(b) shows a line of periodic width, also with $a=14$ mm, fashioned in the same manner as a common low-pass filter. Both structures were

realized with a patterned microstrip line on a homogeneous substrate. In all of the structures used in this study, $d_1=d_2$.

Figure 2(a) shows the measured transmission S-Parameters for a structure from Figure 1(a) made by photolithography on Rogers RO 3003, 1 oz copper board. All measurements in this work were made using a Hewlett-Packard 8719C vector network analyzer with a full 2-port calibration. Copper semi-rigid cable was used to maintain a high quality calibration throughout the transmission line characterization.

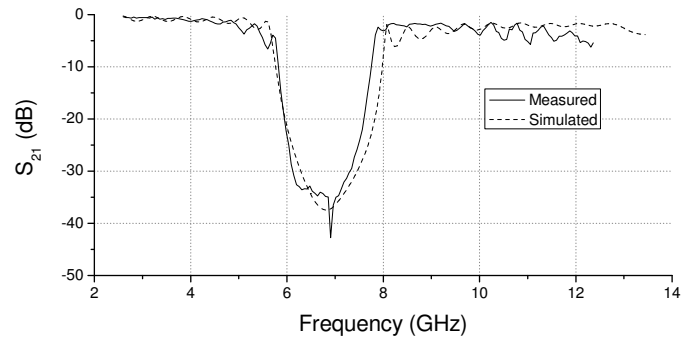


Figure 2a Measured and simulated S_{21} for a transmission line of the design type shown in Figure 1a.

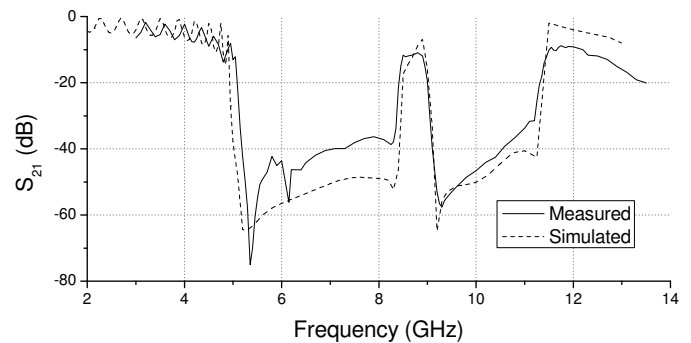


Figure 2b Measured and simulated S_{21} for a transmission line of the design type shown in Figure 1b.

Figure 2(b) shows the measured transmission S-Parameters for a structure similar to Figure 1(b) but made from adhesive copper tape on a 0.040" thick alumina substrate, with a period $a=8.2$ mm. The simulations in Figure 2 used IE3D¹³ and demonstrate the effectiveness of method-of-moments electromagnetic field analysis. However, in the first attempt to simulate the structure in Figure 1b (not shown), all of the features occurred at frequency values that were about 80% of the measured values. To get agreement it was necessary to use $\epsilon_r=6.5$ for the alumina, which is clearly incorrect, but does demonstrate that the effective dielectric constant was roughly 35% lower in practice than would be expected for a pure alumina substrate. Careful examination of the copper tape revealed an approximately 60 μm thick acrylic adhesive layer. Including this layer in the IE3D model above the ground plane and below the microstrip line and setting the alumina permittivity to $\epsilon=9.8$ and the adhesive permittivity to 2.0

produced the simulated curve in Figure 2(b). This illustrates the effect of additional layers on the effective dielectric constant, and further emphasizes the "essential" role observed by Kee¹ played by impedance in the formation of band gaps.

Usually observations of mid-band transmission features, as the one centered at 8.7 GHz in Figure 2b, can be attributed to defects, or in other words point disruptions, of the periodicity¹⁴. However this transmission line included no such irregularities even though the feature is seen both in measurement and in simulation. Direct measurement of the group delay and calculation of the group velocity from the dispersion curve confirm that the half-wavelength at 8.7 GHz is equal to the periodicity of the transmission line. This is also seen in the current distribution in Figure 3 computed with IE3D, providing independent confirmation that the apparent state in the gap is instead a mere suppression of the periodicity.

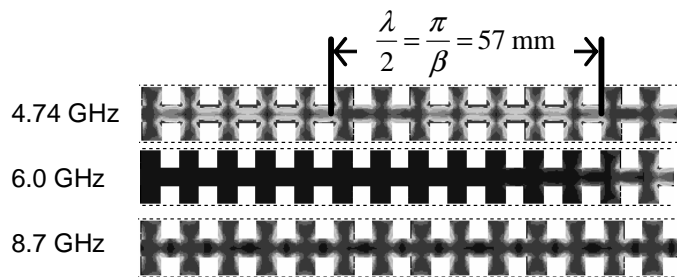


Figure 3 Current distributions on the microstrip line from Figure 2b computed using IE3D outside the PBG (4.74 GHz), inside the PBG (6.0 GHz), and at the in-band allowed state (8.7 GHz). The wavelength at 8.7 GHz is equal to the periodicity of the structure.

Also visible in Figure 2 are oscillatory variations in frequency of the transmission, which occurs in both the magnitude and the delay of the transmission. The frequency separation between peaks is similar to the group velocity divided by twice the line length between the SMA connectors, indicating that these are Fabry-Perot resonances of the quasi-TEM mode between the impedance mismatched ports. The high points of the oscillations correspond to propagation between the ports without loss to the Fabry-Perot mode. The low points correspond to frequencies where there is maximum multiple reflections, producing additional dissipation. Achieving a characteristic impedance outside the PBG of 50 Ω helped to minimize the amplitude of the Fabry-Perot oscillations, as was the case in Figure 2a.

III. DISPERSION

The complex impedance calculated from Equation 3 for the structure in Figure 1a is shown in Figure 4. The real part, $\text{Re}(Z_c)$, goes to 50 Ω outside and away from the PBG. The Fabry-Perot resonances are readily revealed in $\text{Re}(Z_c)$ which is 50 Ω at frequencies where the oscillation in S_{21} is at a peak, indicating that the oscillation depicts dissipative loss of energy

from the TEM mode due to the Fabry-Perot resonance. In several periodic transmission lines, the in-band impedance exhibited explosive growth, possibly even a singularity, at any frequency of almost perfect reflection, where S_{11} was nearly 0 dB accompanied by a 0° phase shift, indicating a soft boundary condition at the device input. The in-band impedance would also sometimes clearly resemble anomalous dispersion, much more evidently than seen in Figure 4, hinting at a possible negative index of refraction. The mechanism which determines the impedance in the high insertion loss regime is not well understood by these authors, and is now a matter of continued investigation.

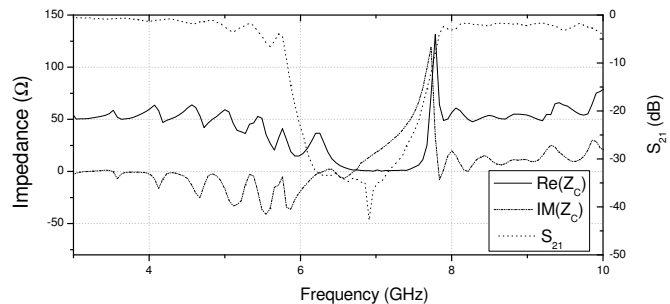


Figure 4 Real and imaginary parts of the characteristic impedance of the transmission line in Figure 1a.

The propagation constant and dispersion curve for a structure similar to that in Figure 1(b) with a lattice parameter $a=14$ mm on 0.030" thick RO3003 circuit board are shown in Figures 5 and 6. The propagation constant, β , was computed from Equation 4. Because of the exponential construction in Equation 4, β is phase wrapped, and a manual unwrapping procedure was applied to β , forcing it to be zero at DC. The dispersion curve constructed in Figure 6, shows the angular frequency, ω , normalized by the lattice parameter, versus the propagation constant times $a/2\pi$. The forbidden band is manifest by a sudden jump in frequency at the Brillouin zone edge ($\beta a/2\pi=0.5$). Because there is some transmission in the PBG, the ideal discontinuity in group velocity at the Brillouin zone edge is in reality continuous and not single valued. However, the expected trend that the group velocity

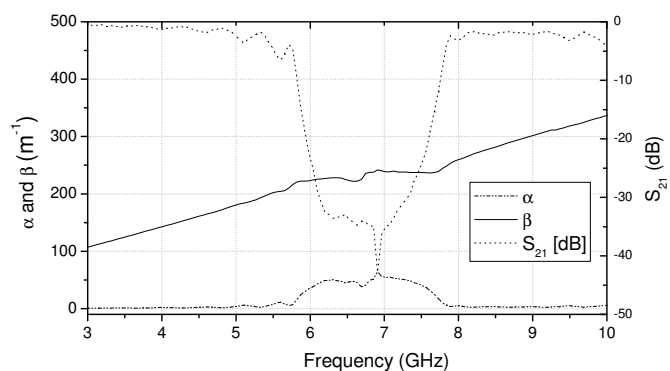


Figure 5 Attenuation coefficient (α) and propagation constant (β) of the transmission line in Figure 1a computed by using measured S-parameter data with Equation 4.

($v_g=d\omega/d\beta$) tends toward zero at the Brillouin zone edge is clearly visible from inspection of the curves in Figure 6.

Alternatively, the dispersion curve can be simulated by using IE3D to prepare plots of the current distribution along the line at various frequencies, such as those shown in Figure 3. The wavelength, λ , is measured directly from the current distributions and is used to compute $\beta=2\pi/\lambda$. Due to the difficulty in accurately identifying wavelengths in the current distribution on visual inspection, this method does not work well for transmission lines with a large impedance contrast, which is why the actual transmission lines in Figure 1 were not used here. Figure 6 shows dispersion curves that were generated using multiple methods: (1) from the current plots; (2) analytically using Equation 2; (3) From IE3D simulated S-Parameters using Equation 4; and (4) from measured S-parameters using Equation 4. With in-band transmission remaining finite, Equation 4 does not result in a perfect discontinuity at the Brillouin zone edge neither with simulated nor with measured S-parameters. Because field simulation shows no current inside the PBG, there is the usual dispersion discontinuity from the simulated current plots. However, the simulated current distribution's offset from the Brillouin zone edge indicates the coarse measure given by field simulated current distribution of the transmission line's dispersive character.

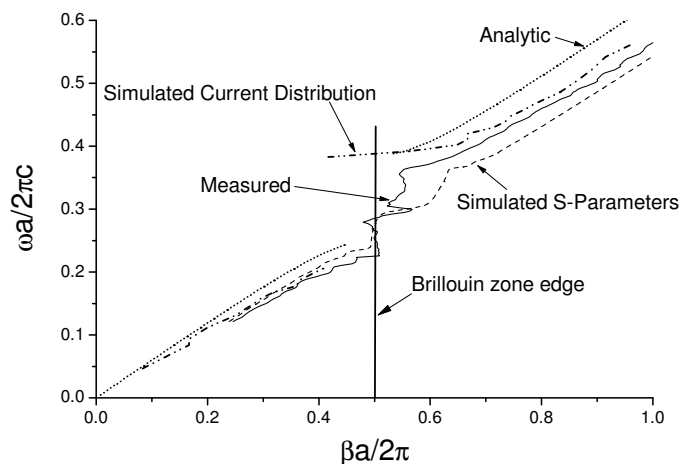


Figure 6 Dispersion curves for a line of the type in Figure 1b determined four different ways. The slope becomes small, and ideally zero, at the edge of the Brillouin zone.

IV. CONCLUSION

Because the S-parameter response of a periodic transmission line has a bandgap with a continuous value of the wavelength at the upper and lower gap edges, dispersion diagrams can be readily determined both experimentally and theoretically. Whether de-embedded from direct measurement, from simulated S-parameters, calculated from simulated current distribution, or computed analytically from Equation 2, PBGs are found, all with similar slopes in the dispersion curves in Figure 6. This work is leading naturally

into the next level of investigation into anomalous dispersion inside the PBG and ultimately to negative index of refraction.

ACKNOWLEDGEMENTS

This work was supported in part by National Science Foundation REU Grant Number 0452206 and by Hope College, Division of Natural and Applied Sciences.

REFERENCES

- ¹ Chul-Sik Kee, Jae-Eun Kim, Hae Yong Park, S.J. Kim, H.C. Song, Y.S. Kwon, N.H. Myung, S.Y. Shin and H. Lim, Essential Parameter in the Formation of Photonic Band Gaps, *Phys Rev E* 59 (1999), 4695-4698.
- ² Mohammad Mojahedi and George V. Eleftheriades, *Dispersion Engineering: The Use of Abnormal Velocities and Negative Index of Refraction to Control Dispersive Effects*, in *Negative-Refraction Metamaterials: Fundamental Principles and Applications*, George V. Eleftheriades and Keith G. Balmain, eds., Wiley Inter-Science, 2005.
- ³ Brian C. Wadell, *Transmission Line Design Handbook*, Artech House Antennas and Propagation Library, 1991.
- ⁴ Rogers Corporation, Rogers, CT, USA.
- ⁵ Part number 836, Compac Corporation, Hackettstown, NJ, USA.
- ⁶ Chul-Sik Kee, Jae-Eun Kim, Hae Yong Park, and H. Lim, Role of Wave Impedance and Refractive Index in Photonic Crystals with Magnetic and Dielectric Properties, *IEEE Trans. Microwave Theo Tech* 47 (1999), 2148-2150.
- ⁷ Eoin O'Reilly, *Quantum Theory of Solids*, Taylor and Francis, 2002.
- ⁸ William R. Eisenstadt and Yungseon Eo, S-Parameter-Based IC Interconnect Transmission Line Characterization, *IEEE Trans. Components, Hybrids and Mfg. Technol.* 15 (1992), 483-490.
- ⁹ Ching-Kuo Wu, Hsien-Shun Wu, Ching-Kuan Cliver Tzuang, Electric-Magnetic-Electric Slow-Wave Microstrip Line and Bandpass Filter of Compressed Size, *IEEE Trans. Microwave Theo Tech* 50 (2002), 1996-2004.
- ¹⁰ Yanyan Zhang and H.Y. David Yang, Ultra Slow-Wave Periodic Transmission Line Using 3D Substrate Metallization, *Proceedings of the 2008 International Microwave Symposium*, Atlanta, GA, June 15-20, 2008.
- ¹¹ A. Saib, R. Platteborze and I Huynen, Experimental Demonstration of the Origin of Photonic Bandgap Creation and Associated Defect Modes in Microwave Planar Circuits, *Microwave Opt Technol Lett* 41 (2004), 5-9.
- ¹² Manoj K. Tiwari, K.K. Gupta, H.C. Gupta and D.C. Dube, "Photonic Band Gap Studies on Periodic Metallic Structures in the Microwave Region," *Microwave and Optical Technol. Lett*, v. 35, no. 6, December 20, 2002, pp. 483-486.
- ¹³ Zeland Software, Fremont, CA, USA.
- ¹⁴ E. Yablonovitch, T.J. Gmitter, R.D. Meade, A.M. Rappe, K.D. Brommer, and J.D. Joannopoulos, Donor and Acceptor Modes in Photonic Band Structures, *Phys. Rev Lett* 67 (1991), 3380-3383.